Green light emission from terbium doped silicon rich silicon oxide films obtained by plasma enhanced chemical vapor deposition

2012 Nanotechnology 23 475707

(http://iopscience.iop.org/0957-4484/23/47/475707)

Nanotechnology **23** (2012) 475707 (8pp) doi:10.1088/0957-4484/23/47/475707

Green light emission from terbium doped silicon rich silicon oxide films obtained by plasma enhanced chemical vapor deposition

A Podhorodecki[1], G Zatryb[1], J Misiewicz[1], J Wojcik[2], P R J Wilson[2] and P Mascher[2]

[1] Institute of Physics, Wroclaw University of Technology, Wybrzeze Wyspianskiego 27, 50-370 Wroclaw, Poland
[2] Department of Engineering Physics and Centre for Emerging Device Technologies, McMaster University, 1280 Main Street W, Hamilton, ON L8S 4L7, Canada

E-mail: artur.p.podhorodecki@pwr.wroc.pl

Received 6 July 2012, in final form 2 September 2012
Published 30 October 2012
Online at stacks.iop.org/Nano/23/475707

Abstract
The effect of silicon concentration and annealing temperature on terbium luminescence was investigated for thin silicon rich silicon oxide films. The structures were deposited by means of plasma enhanced chemical vapor deposition. The structural properties of these films were investigated by Rutherford backscattering spectrometry, transmission electron microscopy and Raman scattering. The optical properties were investigated by means of photoluminescence and photoluminescence decay spectroscopy. It was found that both the silicon concentration in the film and the annealing temperature have a strong impact on the terbium emission intensity. In this paper, we present a detailed discussion of these issues and determine the optimal silicon concentration and annealing temperature.

S Online supplementary data available from stacks.iop.org/Nano/23/475707/mmedia

(Some figures may appear in colour only in the online journal)

1. Introduction

Silicon rich silicon oxide (SRSO) structures have attracted considerable attention in recent years due to their interesting optical properties. Research on these materials has been additionally stimulated by potential applications such as visible light emission from electrically excited silicon nanocrystals [1] (Si-NC), silicon-based lasers [2], third generation photovoltaics [3] and non-volatile memory devices [4]. The major advantage of SRSO structures are their full compatibility with complementary metal–oxide–semiconductor technology, which could lead to easy integration with various microelectronic devices. Research has also been conducted on materials where the SRSO matrices are doped with other optically-active elements, such as lanthanide ions [5]. Most effort in this field has been directed towards erbium [6] and neodymium [7] doped SRSO, due to emission wavelengths that are important for telecommunications applications. As a result of the research, Er^{3+}/Si-NC light-emitting diodes (LEDs) with 10% efficiency have been reported [8]. Considerable attention has also been paid to europium [9] and cerium [10] doped SRSO structures due to potential applications as red and blue light emitters and in solid state lighting, respectively. From the point of view of applications in multicolor LEDs it is therefore interesting to explore the possibility of obtaining efficient green light emission from terbium (Tb) doped SRSO materials. At the moment, this problem has been given at most moderate attention, focused mainly on Tb doped stoichiometric SiO_2 [11] and oxygen rich silicon oxide (ORSO) matrices [10]. In this work we

examine the structural and optical properties of Tb doped SRSO matrices.

As for most of the trivalent lanthanide ions, Tb^{3+} emission arises from transitions within the 4f shell of the ions. These transitions are parity forbidden, leading to very low absorption cross sections ($\sim 10^{-21}$ cm^2) and it is thus difficult to obtain efficient emission from the ions. However, if the rare-earth ion is placed at a site which lacks inversion symmetry (e.g. embedded in a matrix) a mixing of opposite-parity states of the $4f^{(n-1)}5d$ configuration into the $4f^n$ states can occur, significantly increasing the intensity of transitions between the levels. Beside this, a few different mechanisms that may enhance emission of Tb ions in a matrix have been considered. These are, in particular, energy transfer from Si-NC to Tb^{3+} ions or oxygen-mediated excitation of the lanthanide. The latter mechanism was found to play a significant role in the case of ORSO matrices [10], where Tb^{3+} ions can be easily coordinated by oxygen atoms. However, in the case of SRSO matrices, there are still many open questions regarding the actual ion excitation and relaxation mechanism as well as the relation between the deposition parameters and the material's microscopic structure. The following sections will address these issues.

2. Experimental details

Terbium doped SRSO thin films were grown on ⟨100⟩ Si substrates by electron cyclotron resonance plasma enhanced chemical vapor deposition (ECR-PECVD). The silicon and oxygen precursors were silane (30% SiH_4 in Ar) and O_2 (10% O_2 in Ar), respectively. The oxygen flow rate was varied between 4 and 25 sccm in order to obtain samples with various Si concentrations. Additional Ar gas was added to the plasma region in order to maintain the same deposition pressure of 2.1 mTorr for the undoped samples, and 2.5 mTorr for Tb doped samples, respectively. The beta-diketonate organic compound tris(2,2,6,6-tetramethyl-3,5-heptanedionato)-Tb(III) ($Tb(tmhd)_3$), was used as the Tb precursor. The Tb diffusion cell was heated up to 120 °C within a manifold to sublime the precursor and introduce it into the chamber alongside the silane, using Ar as the carrier gas. The Ar carrier gas flow was set constant at 5 sccm. During the deposition process the substrate stage was heated to a temperature of 350 °C, resulting in a surface temperature of the sample of 120 °C. Substrate rotation of 20 r.p.m. was used to achieve uniformity and homogeneity of the films. In the post-deposition process the samples were cleaved into smaller pieces and annealed at temperatures (T_a) from 600 to 1200 °C in a quartz tube furnace under flowing N_2. Further details of the deposition system, film growth, and structure have been discussed previously [12].

Variable angle spectroscopic ellipsometry (VASE) was employed in order to determine the optical constants and thicknesses of the thin films. Ellipsometry is a very sensitive surface and thin film measurement technique that uses polarized light. It measures the change in the polarization state of light reflected from the surface of a sample. The measured values are expressed as ψ and δ. These values are related to the ratio of Fresnel reflection coefficients, for p- and s-polarized light, respectively. The Cauchy and Tauc–Lorentz dispersion relations were used for the determination of the optical constants of the deposited thin films. The former was mainly used for stoichiometric or slightly non-stoichiometric SiO_2 films, while the latter was employed for films with a higher silicon content [13, 14]. A VASE M-2000 ellipsometer (J A Woollam) operating in the wavelength range of 240–1700 nm was used in this project.

Film compositions were determined through Rutherford backscattering spectrometry (RBS) experiments conducted in the Tandetron Accelerator Laboratory at the University of Western Ontario using 1.0 MeV $^4He^+$ ions with an incident angle θ of 3° and random rotation of ϕ to minimize substrate channeling. The atomic concentrations of elements (excluding hydrogen) as a function of depth in the film were calculated by fitting the RBS data using the QUARK simulation package after calibrating the experimental parameters against a reference sample consisting of a known dose of bismuth implanted into a silicon wafer [15]. Details of the film structure were investigated via cross-sectional high resolution transmission electron microscopy (TEM) and scanning transmission electron microscopy (STEM) using a FEI Titan 80–300 Cryo-*in situ* microscope at the Canadian Centre for Electron Microscopy (CCEM) at McMaster University. The same instrument was also used to obtain compositional information for different features within the TEM images through the use of x-ray energy dispersive spectroscopy (XEDS).

Room temperature micro-Raman scattering was measured using a single-stage spectrometer (T64000 Horiba Jobin Yvon) equipped with a liquid nitrogen cooled silicon charge-coupled device camera. An Ar^+ laser ($\lambda = 514.5$ nm) was used as the excitation source. The measurements were performed in VH polarization. The photoluminescence (PL) was measured using a pulsed laser excitation source ($\lambda_{EXC} =$ 266 nm) and a photomultiplier tube detector. The PL decay was measured using pulsed laser excitation ($\lambda_{EXC} = 266$ nm) coupled to a gated detection system (QuantaMaster from Photon Technology International).

3. Structural properties

In the present study, we examined Tb^{3+} doped SRSO structures that differed in terms of Si concentration and annealing temperature. As determined from ellipsometry measurements, the average thickness of the investigated films was 205 nm. Moreover, the refractive indices (n) obtained for samples with various Si concentrations were 1.47, 1.55, 1.69 and 2.02 (at $\lambda = 632.8$ nm). The increase in the refractive index is due to increasing Si concentration in the films. This was confirmed by RBS. The total Si concentration determined for the investigated SRSO films is 33 at.% (almost stoichiometric SiO_2), 35, 39 and 50 at.%, obtained for samples with $n = 1.47$, 1.55, 1.69 and 2.02, respectively. The RBS experiments also show that the Si concentration does not change measurably after annealing.

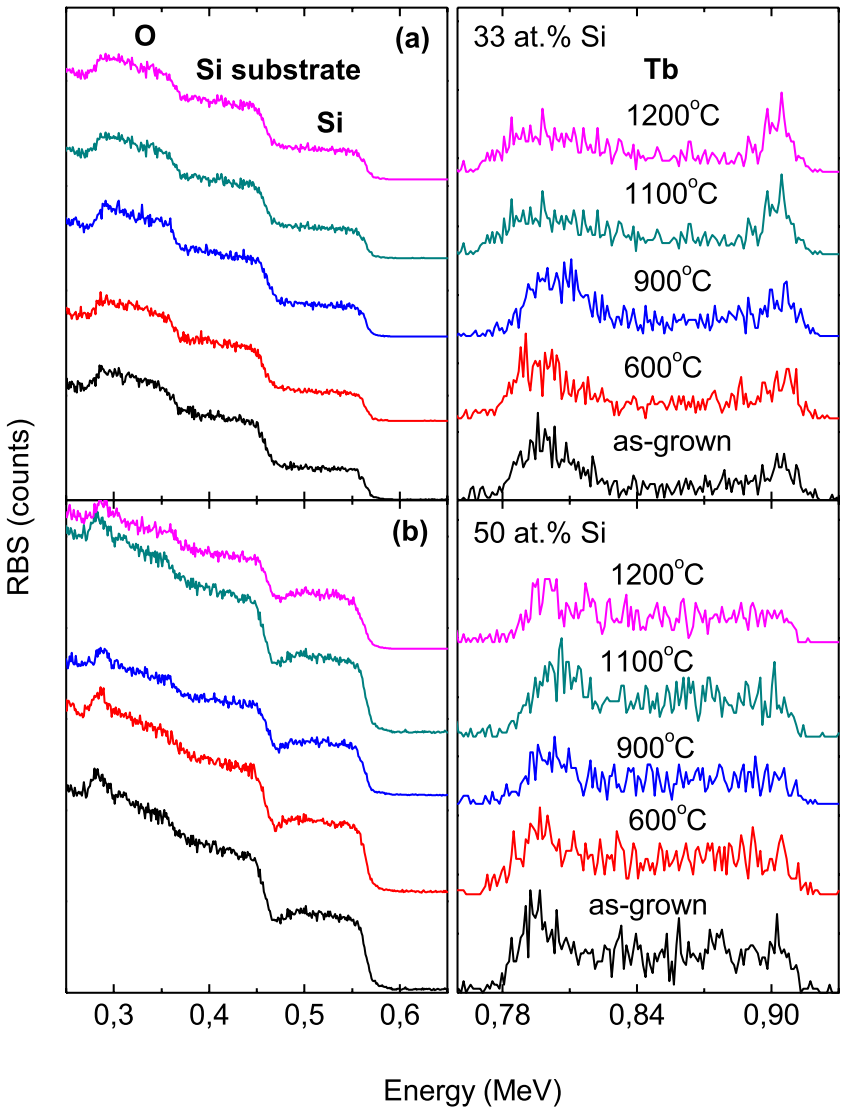

Figure 1. RBS spectra of samples with (a) 33 at.% Si and (b) 50 at.% Si, annealed at different temperatures. The spectra have been arbitrarily up-shifted for clarity. The panels on the right show the RBS signal related to Tb in the SRSO film. The distribution of energy of the backscattered ions corresponds to Tb located at different depths in the film. The high-energy edge of the spectra is related to backscattering from Tb at the surface of the film and cumulative energy losses occur for ions penetrating deeper into the film. The panels on the left show the RBS signal related to Si substrate as well as Si and O elements in the SRSO film.

The RBS results obtained for as-grown and annealed samples, containing 33 and 50 at.% Si are shown in figures 1(a) and (b), respectively. The low-energy part of the spectra, below 0.6 MeV, corresponds to backscattering from Si and O atoms in the film and Si atoms in the substrate while the high-energy part of the spectra, between 0.78 and 0.93 MeV, is related to backscattering from Tb ions in the SRSO films (see the supplementary data file for details; available at stacks.iop.org/Nano/23/475707/mmedia). The Tb concentration estimated from the RBS spectra is below 0.1 at.% for all the samples and it does not vary measurably with annealing temperature and Si concentration in the films.

Figure 1 also shows that, in the case of as-grown samples, the Tb ions are generally non-uniformly distributed through the film thickness (see the supplementary data file for details; available at stacks.iop.org/Nano/23/475707/mmedia). As indicated by peaks in the RBS spectra, a significant number of the Tb ions tend to agglomerate close to the film/substrate and film/air interfaces. As a result, for as-grown samples the Tb concentration is higher at the film boundaries than in the bulk of the film. It can be also seen that depending on the Si concentration in the film, annealing of the samples at high temperatures has a different impact on the Tb distribution across the film thickness. For the 50 at.% samples we observe Tb diffusion from the film interfaces towards the center of the film. For samples annealed above 900 °C, the Tb distribution becomes almost uniform across the film depth. This is exactly what we would expect, since in general diffusion is driven by concentration gradients and the diffusive flux is directed opposite to the concentration gradient. However, in the case of 33 at.% Si samples the situation seems to be different. Figure 1(a) shows that annealing makes the Tb distribution across the films slightly more uniform, but even at 1200 °C

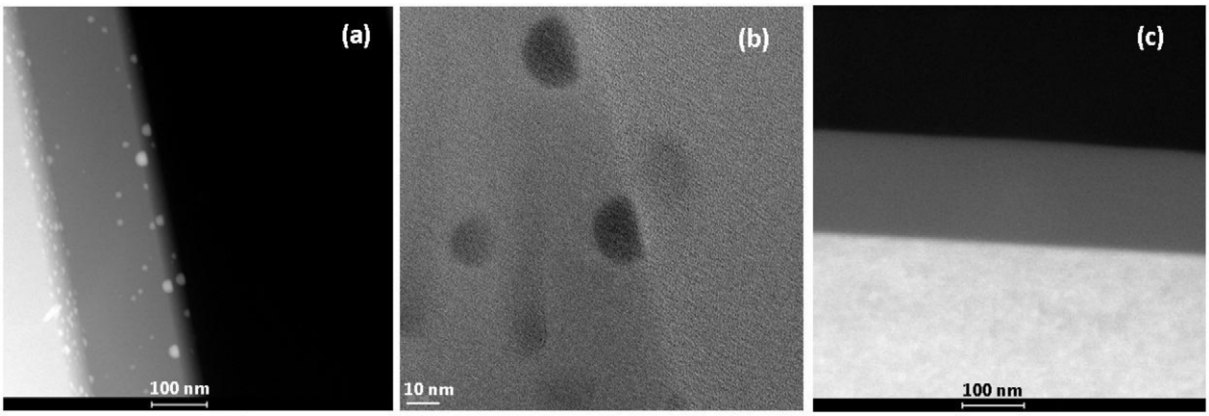

Figure 2. TEM images of samples with (a), (b) 33 at.% Si (cross-sectional STEM and in-plane TEM, respectively) and (c) 50 at.% Si (cross-sectional STEM), all annealed at 1200 °C.

a significant fraction of the Tb ions remains located close to the film interfaces. Since in the case of 33 at.% Si samples the initial concentration gradient (in as-grown samples) is even higher than in the case of 50 at.% Si samples, we may conclude that the Tb diffusivity is lower for SRSO films with low Si concentrations.

Figure 2(a) shows a cross-sectional STEM image measured for a 33 at.% Si sample annealed at 1200 °C. Based on the RBS results and XEDS analysis (see the supplementary data file for details; available at stacks.iop.org/Nano/23/475707/mmedia) at different points in the TEM image, the bright spots visible against the dark-gray SRSO film region can be identified as Tb agglomerates. At points corresponding to the agglomerates, XEDS measurements yielded Tb concentrations of up to 2 at.% whereas the concentration in other regions of the film were below the sensitivity limit of the XEDS detector. The size of the Tb agglomerates varies from a few to tens of nanometers. Moreover, figure 2(b) shows an in-plane TEM image of these Tb clusters. The clusters do not reveal any visible crystal structure. At present it is also not completely clear if the clusters are composed of Tb alone and/or of Tb oxide. It was, however, proposed that in SiO_2 the oxidized form of Tb clusters is thermodynamically favorable. For example, the standard enthalpy of formation (at 298 K) of Tb_2O_3 is more negative (the process is more exothermic) than that of SiO_2 [9]. Since in the SRSO matrix Tb atoms compete with Si atoms to bond with oxygen, a lower enthalpy of formation suggests that the oxygen is favorably bonded to Tb atoms over Si atoms.

What is more, figure 2(c) shows a cross-sectional TEM image measured for a 50 at.% Si sample annealed at 1200 °C. Clearly, due to diffusion, Tb atoms have spread uniformly in the film and no Tb agglomerates can be seen in this case. Altogether, the obtained results indicate that agglomeration of Tb atoms in the form of clusters strongly depends on the Si concentration and is inefficient in SRSO films of high Si content. Assuming that the Tb clusters are present in oxidized form, we may explain this effect by the lower probability of finding oxygen atoms in the vicinity of Tb atoms in films of high Si concentration. On the other hand, when the Si atom content is low compared to O atoms, the probability of finding Tb and O atoms close to each other increases and Tb agglomerates are formed efficiently.

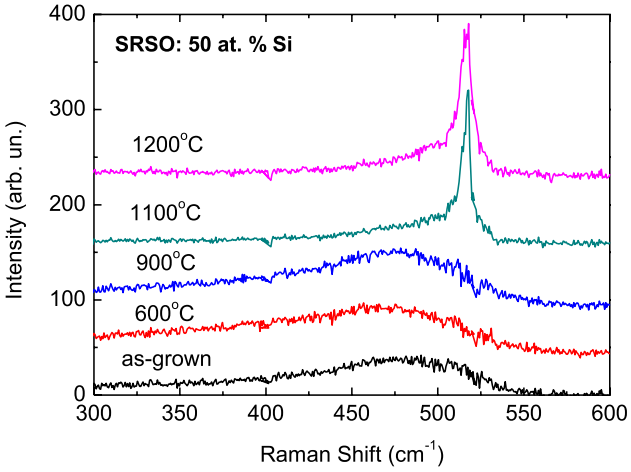

Figure 3. Raman spectra obtained for as-grown and annealed samples with 50 at.% Si.

Finally, figure 3 shows Raman spectra measured for 50 at.% Si samples annealed at different temperatures, up to 1200 °C. It can be seen that up to 900 °C, the only Raman signal is related to amorphous Si (a-Si) present in the film (a broad peak centered around 470 cm^{-1}) [16]. For samples annealed at 1100 and 1200 °C a peak centered at around 520 cm^{-1} appears, confirming the presence of Si-NCs [17]. It should be noted here that for the rest of the investigated samples we were not able to detect any Raman signal related to a-Si or Si-NCs. This is, however, not surprising since the amount of excess Si in these samples is very low, probably below our detection limit. Nevertheless, the most important conclusion to be drawn is that the major modifications of the matrix structure (i.e. crystallization of the excess Si) takes place for annealing temperatures significantly exceeding 900 °C.

4. Optical properties and discussion

The room temperature PL spectra of the SRSO:Tb^{3+} films obtained for an excitation wavelength of $\lambda_{EXC} = 266$ nm (resonant with the 4f–5d transition of Tb^{3+} ions) are shown in figure 4 as a function of the Si concentration for samples annealed at 1200 °C. For each sample, four main PL bands can be seen that originate from radiative transitions between intra-4f energy levels of Tb^{3+} ions. The observed transitions are $^5D_4$–$^7F_6$ (485 nm), ^{5}D4–$^7F_5$ (540 nm), ^{5}D4–$^7F_4$ (588 nm) and ^{5}D4–$^7F_3$ (620 nm) [18], with the $^5D_4$–$^7F_5$ transition being the most intense. Moreover, in the case of the 35 at.% Si sample, some high-energy emission bands are clearly visible, which can be assigned to the $^5D_3$–$^7F_6$ (376 nm), $^5D_3$–$^7F_5$ (411 nm) and $^5D_3$–$^7F_4$ (434 nm) transitions of Tb^{3+} ions [18]. These transitions can also be observed for the 33 at.% Si sample, but in this case the emission intensity is very weak. For the 39 and 50 at.% samples the blue lines disappear. It should be mentioned here that the absence of the blue emission lines between 370–480 nm is characteristic for efficient non-radiative transition from $^5D_3$ to $^5D_4$ promoted by the presence of, for example, the OH^- mode (3450 cm^{-1}), which is almost in resonance with the energy gap between the $^5D_3$ and $^5D_4$ levels of Tb^{3+} [19]. It may suggest that coupling to OH^- modes is efficient in the samples with 39 and 50 at.% Si. On the other hand, the blue emission may be also be quenched by cross relaxation between neighboring Tb^{3+} ions [19]. For SiO_2 matrices it has been shown that this effect may play a role when the Tb concentration exceeds 0.5 at.% [11]. In our case, the Tb concentration is very low and therefore we may rather exclude the ion–ion interactions.

Another interesting feature that can be observed in figure 4 is the presence of a broad PL band between 350 and 700 nm in the case of the 50 at.% Si sample. This band may be related to the presence of Si-NCs [20] which was confirmed in the case of the 50 at.% Si sample by Raman spectroscopy. On the other hand there are some oxide defects that exhibit PL in the visible range that also may be responsible for the observed emission band [21]. Therefore, at the moment the origin of the broad PL band observed in the case of the 50 at.% Si sample is not fully understood.

Figure 5(a) shows the PL intensity of the main $^5D_4$–$^7F_5$ transition as a function of the Si concentration in the SRSO films annealed at 1200 °C. It can be seen that addition of excess Si to the film significantly enhances the ^{5}D4–$^7F_5$ emission. The strongest PL was obtained for the 35 at.% Si sample.

To investigate the $^5D_4$–$^7F_5$ emission in more detail, we measured PL decays at $\lambda_{EM} = 540$ nm using the excitation wavelength $\lambda_{EXC} = 266$ nm. In general, the obtained dependences are of single exponential nature and can be characterized by a decay time constant τ_{PL}. The extracted τ_{PL} values are shown in figure 5(b) as a function of the Si concentration. Clearly, increase in the Si concentration results in a decrease in the PL lifetime. We can, however, divide the obtained data into two concentration regimes. For Si concentrations between 35 and 50 at.% the decrease in τ_{PL} correlates with a decrease in the PL intensity I_{PL}.

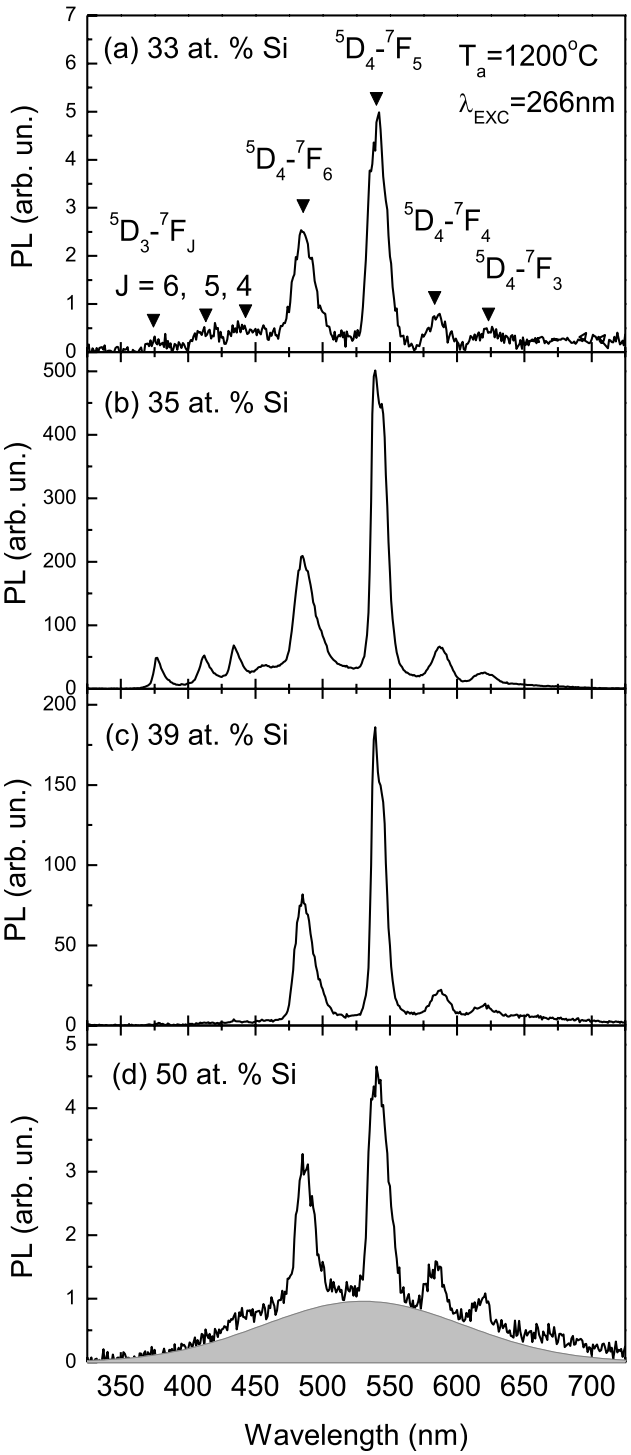

Figure 4. Photoluminescence spectra of SRSO:Tb^{3+} films annealed at 1200 °C shown as a function of the Si concentration.

Taking into account the simplest model where $I_{PL} \sim N^*/\tau_{PL}$ and $1/\tau_{PL} = 1/\tau_R + 1/\tau_{NR}$ (with τ_R and τ_{NR} being the radiative and non-radiative decay times, respectively, and N^* being the number of emitting ions), the observed correlation may be related to an increased non-radiative recombination rate ($1/\tau_{NR}$) in samples with higher Si concentrations. This correlates with a decrease in PL intensity because of an increase in the number of new non-radiative centers.

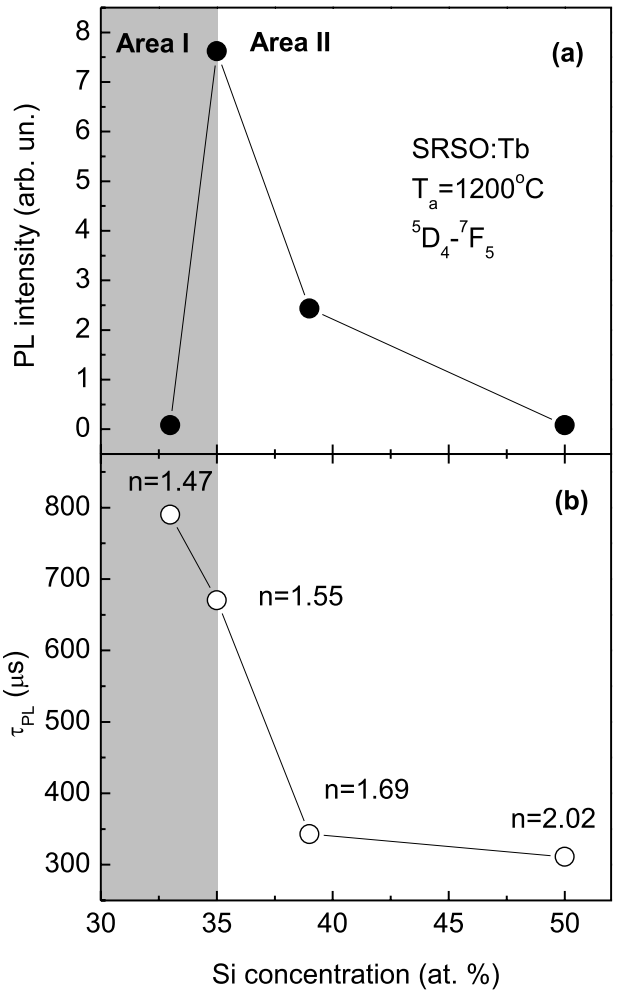

Figure 5. Photoluminescence intensity (top panel) and photoluminescence lifetime (bottom panel) shown as a function of the Si concentration for samples annealed at 1200 °C.

Additionally, another mechanism should also be considered to explain the decrease in emission decay times observed in figure 5(b). According to the Judd–Ofelt theory [22], the radiative recombination rate ($f = 1/\tau_R$) of an optical transition is an increasing function of the refractive index of a medium surrounding the ion according to following equation:

$$f = \frac{1}{\tau_R} \propto n\left(\frac{n^2+2}{3n}\right)^2 \sum_{l=2,4,6} \Omega_l |\langle \varphi_a | U^{(l)} | \varphi_b \rangle|^2 \qquad (1)$$

where n is the refractive index of the matrix, φ_a and φ_b are the initial and final states of single parity, $U^{(l)}$ is the irreducible tensor form of the dipole operator, λ is the emission wavelength and Ω_l are the Judd–Ofelt parameters, describing the local environment of the ion.

Therefore, when the Si concentration in the film increases, we expect to observe a decrease in the PL lifetime and a simultaneous increase in the PL intensity, since the refractive index increases. Indeed, this effect was observed, when the Si concentration increased from 33 to 35 at.% (the region indicated as Area I in figure 5). However, for concentrations exceeding 35 at.% Si, the observed decrease in τ_{PL} is not accompanied by an increasing PL intensity, suggesting that non-radiative recombination dominates at high Si concentrations (region indicated as Area II in figure 5). Therefore, 35 at.% Si seems to be an optimal concentration, where non-radiative processes are not yet very efficient and the radiative recombination rate is still sufficiently high to obtain fairly good emission properties.

Moreover, since silicon is a less electronegative element than oxygen we expect the SRSO matrix to become more covalent at higher Si concentrations. On the other hand, it is well known that the electron–phonon coupling strength increases as the Tb environment becomes more covalent [23]. Therefore, electron–phonon coupling may be one of the non-radiative recombination mechanisms responsible for PL quenching (i.e. coupling to OH^- modes). This hypothesis can be supported by the fact that the blue emission lines between 350 and 450 nm disappear in the case of the 39 and 50 at.% samples, where the non-radiative recombination is especially effective. Another possibility is that the non-radiative recombination is due to coupling between defect states and Tb ion levels (energy-transfer mechanism). We cannot exclude that, at least partially, this kind of process leads to shortening of the PL lifetime and a decrease in the PL intensity.

Figure 6 shows photoluminescence spectra obtained for samples with 35 at.% Si annealed at different temperatures (up to 1200 °C). Similar to the samples with different Si concentrations, the obtained spectra display the characteristic emission of a Tb^{3+} ion composed of four bands associated with the $^5D_4$–^7F_j transitions ($j = 6, 5, 4, 3$) and three bands associated with $^5D3$–^7F_i transitions ($i = 6, 5, 4$). For each annealing temperature, the emission is dominated by the green band centered at 540 nm ($^5D_4$–$^7F_5$), followed by the band centered at 485 nm ($^5D4$–$^7F_6$).

Moreover, figure 6 demonstrates that $^5D3$–^7F_i transition bands are present for all of the annealing temperatures. This may indicate a lack of significant ion–ion interactions that could quench these transitions. However, it can be also seen that the blue bands between 370 and 480 nm change significantly as a function of the annealing temperature. For the as-grown sample the bands are wide and almost merged together. When the annealing temperature increases the full width at half maximum (FWHM) of the bands decreases, and starting from $T_a = 900$ °C the bands become well resolved. Since these transitions are sensitive to the crystal field around the ion, this result indicates that annealing temperature changes the structural environment of the Tb^{3+} ions.

Figure 7(a) shows that for the 35 at.% Si sample increasing the annealing temperature results in a significant enhancement of the PL intensity (at $\lambda_{EM} = 540$ nm). The slight deviation from this trend observed for $T_a = 900$ °C is due to a slightly stronger blue emission than in other cases (the ratio of blue/green emission for $T_a = 900$ °C is almost twice as high as in the case of the rest of the samples). Figure 7(b) shows the dependence of the PL lifetime on the annealing temperature obtained for a 35 at.% Si concentration. It can be seen that the PL lifetime increases as a function of T_a up to 900 °C and then rapidly decreases.

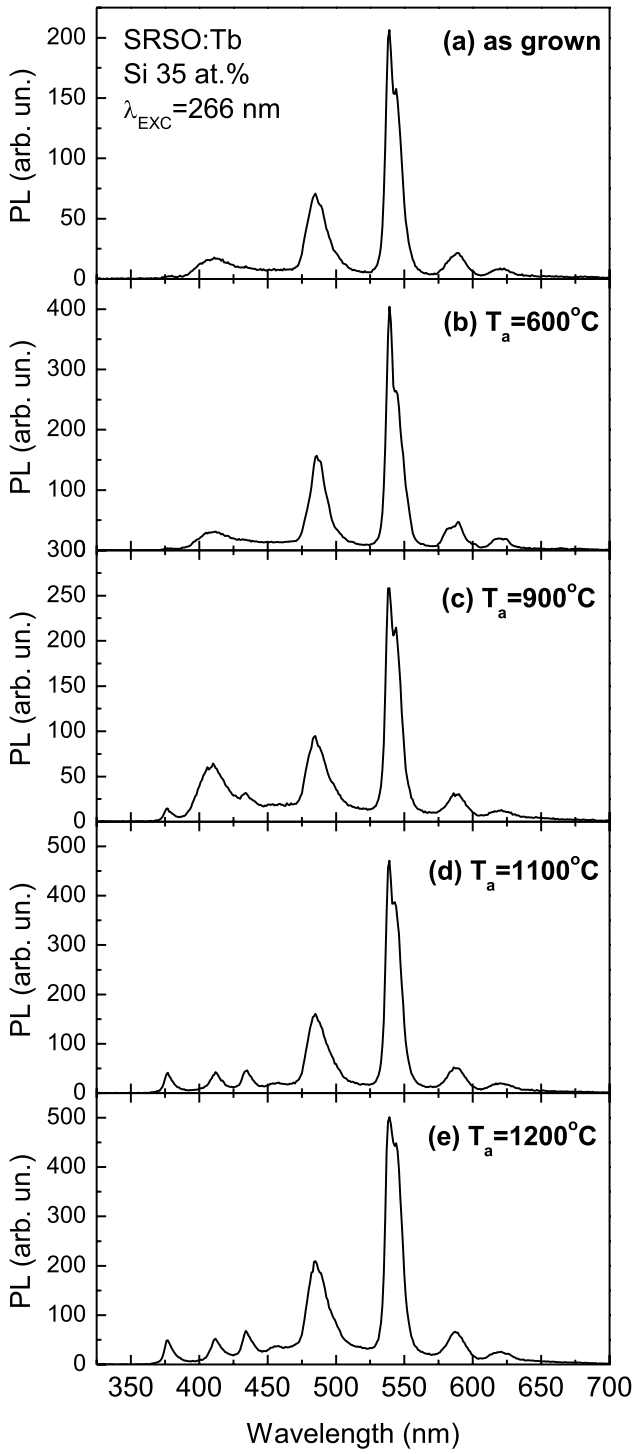

Figure 6. Photoluminescence spectra of SRSO:Tb^{3+} films with 35 at.% Si shown as a function of the annealing temperature.

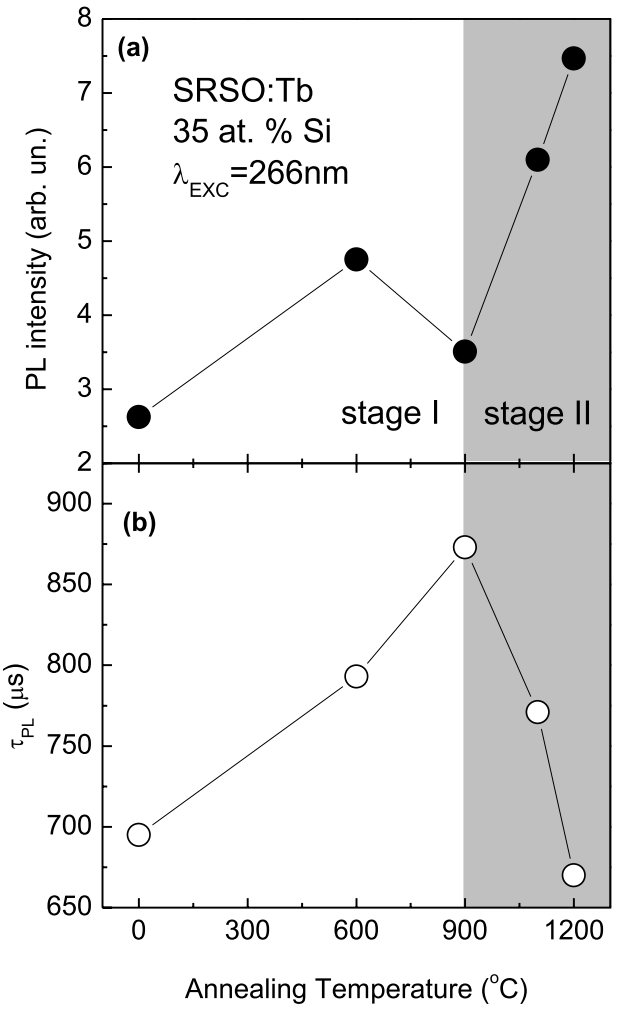

Figure 7. Photoluminescence intensity (^{5}D4–$^7F_5$ band) and photoluminescence lifetime shown as a function of the annealing temperature for SRSO:Tb^{3+} films with 35 at.% Si.

To explain the obtained results we should consider the influence of two different effects: (1) reduction of non-radiative recombination centers at early stages of annealing (stage I in figure 7) and (2) increasing oscillator strength of the $^5D_4$–$^7F_5$ transition at higher annealing temperatures (stage II in figure 7). The reduction of non-radiative recombination could be due to reduction of the defect states which are annihilated during annealing up to 900 °C. This results in a simultaneous increase of the PL intensity and PL lifetime (since the non-radiative recombination rate $1/\tau_{NR}$ is reduced). The reduction of non-radiative recombination induced by annealing is the dominating effect for temperatures up to 900 °C (stage I). Another result of the annealing is matrix crystallization. As shown by the Raman measurements (figure 3) the most significant structural changes of the matrix occur starting from $T_a = 1100$ °C. Therefore, we expect significant modifications of the Tb environment after annealing at high temperatures, exceeding 900 °C. These structural changes may influence the crystal field surrounding the ions, for example lowering its symmetry. In general, the 4f–4f transitions are forbidden due to selection rules. However, if the crystal field becomes more non-centrosymmetric the optical transitions become more allowed which leads to increased oscillator strength. Therefore, the change in the structural environment of the Tb ions becomes the dominant effect which leads to the observed decrease in the PL lifetime and simultaneous increase in the PL intensity, for annealing temperatures between 900 and 1200 °C (stage II).

Conclusions

Terbium doped SRSO films were deposited by means of ECR-PECVD. The influence of the Si concentration and annealing temperature on the emission properties was investigated. It was shown that the examined materials exhibit visible PL with a maximum intensity at 540 nm, originating from intra-4f transitions of Tb^{3+} ions. It was found that the PL intensity strongly depends on the Si concentration in the SRSO film. An increase in the Si concentration influences the emission properties in two ways. First of all, the refractive index of the film increases which enhances the oscillator strength of the optical transitions. On the other hand, the non-radiative recombination also increases, limiting the PL intensity. Therefore, from the point of view of emission efficiency, the optimal Si concentration in the film is about 35 at.% Si. Besides the Si concentration, another effect investigated in this work was the influence of the annealing temperature on Tb^{3+} emission. It was found that the PL intensity increases as a function of the annealing temperature. This effect was ascribed to the structural changes of the SRSO matrix. At early stages of the annealing (up to 900 °C) the most important factor enhancing the PL intensity is a reduction in the number of non-radiative recombination centers. However, as shown by Raman measurements, starting from $T_a = 1100$ °C structural changes occur in the matrix (crystallization) and the Tb environment changes. Therefore, the further increase in the PL intensity obtained for high annealing temperatures (1100–1200 °C) can be ascribed to the increasing oscillator strength of the intra-4f transitions, induced by the change of the crystal field around the ions.

Acknowledgments

The authors would like to thank Connor Wilson at McMaster University for his help preparing samples for TEM imaging, Andreas Korinek from the Canadian Centre for Electron Microscopy at McMaster University for his assistance in capturing the TEM images, and Jack Hendriks from the Tandetron Accelerator Laboratory at the University of Western Ontario for his assistance in conducting the Rutherford backscattering spectrometry measurements. AP would like to acknowledge financial support from the Iuventus Plus program (no. IP2011 042971). In Canada, the work was supported by the Natural Sciences and Engineering Research Council of Canada (NSERC) under the Discovery Grants Program. The Raman spectral measurements were conducted as a part of the NLTK project (POIG. 02.02.00-00-003/08-00).

References

[1] Huh C, Kim K, Kim B K, Kim W, Ko H, Choi C and Sung G Y 2010 *Adv. Mater.* **22** 5058–62
[2] Pavesi L, Dal Negro L, Mazzoleni C, Franzo G and Priolo F 2000 *Nature* **408** 440–4
[3] Perez-Wurfl I, Hao X, Gentle A, Kim D-H, Conibeer G and Green M A 2009 *Appl. Phys. Lett.* **95** 153506
[4] Feng T, Yu H, Dicken M, Heath J R and Atwater H A 2005 *Appl. Phys. Lett.* **86** 033103
[5] Makarova M, Sih V, Warga J, Li R, Dal Negro L and Vuckovic J 2008 *Appl. Phys. Lett.* **92** 161107
[6] Savchyn O, Coffey K R and Kik P G 2010 *Appl. Phys. Lett.* **97** 201107
[7] Debieu O, Bréard D, Podhorodecki A, Zatryb G, Misiewicz J, Labbé C, Cardin J and Gourbilleau F 2010 *J. Appl. Phys.* **108** 113114
[8] Heitmann J, Müller F, Zacharias M and Gösele U 2005 *Adv. Mater.* **17** 795–803
[9] Nazarov A N, Tiagulskyi S I, Tyagulskyy I P, Lysenko V S, Rebohle L, Lehmann J, Prucnal S, Voelskow M and Skorupa W 2010 *J. Appl. Phys.* **107** 123112
[10] Roschuk T, Wilson P R J, Li J, Zalloum O H Y, Wojcik J and Mascher P 2010 *Phys. Status Solidi* b **247** 248–53
[11] Amekura H, Eckau A, Carius R and Buchal C 1998 *J. Appl. Phys.* **84** 3867–71
[12] Boudreau M, Boumerzoug M, Mascher P and Jessop P E 1993 *Appl. Phys. Lett.* **63** 3014
[13] Amans D, Callard S, Gagnaire A, Joseph J, Ledoux G and Huisken F 2003 *J. Appl. Phys.* **93** 4173
[14] Chen T P, Liu Y, Tse M S, Ho P F, Dong G and Fung S 2002 *Appl. Phys. Lett.* **81** 4724
[15] Lennard W N 2012 The QUARK simulation package for RBS is available from the author at wlennard@uwo.ca
[16] Khriachtchev L, Kilpelä O, Karirinne S, Keränen J and Lepistö T 2001 *Appl. Phys. Lett.* **78** 323
[17] Zatryb G, Podhorodecki A, Hao X J, Misiewicz J, Shen Y S and Green M A 2011 *Nanotechnology* **22** 335703
[18] Podhorodecki A, Nyk M, Misiewicz J and Strek W 2007 *J. Lumin.* **126** 219–24
[19] Romero V H, De La Rosa E, López-Luke T, Salas P and Angeles-Chavez C 2010 *J. Phys. D: Appl. Phys.* **43** 465105
[20] Zatryb G, Podhorodecki A, Hao X J, Misiewicz J, Shen Y S and Green M A 2010 *Opt. Express* **18** 22004–9
[21] Zhu M, Chen G i and Chen P 1997 *Appl. Phys.* A **65** 195–8
[22] Walsh B M 2006 *Advances in Spectroscopy for Lasers and Sensing* ed B D Bartolo and O Forte (The Netherlands: Springer) pp 403–33
[23] de Mello Donega C, Meijerink A and Blasse G 1992 *J. Phys.: Condens. Matter* **4** 8889–902